Qu *et al.*
Acta Neuropathologica Communications (2024) 12:179
https://doi.org/10.1186/s40478-024-01890-0

Acta Neuropathologica Communications

RESEARCH

Open Access

Inhibition of RtTg neurons reverses methamphetamine-induced attention deficits

Xiaotian Qu[1,2], Pingyuan Yang[3], Rongwei Zhai[4*] and Zhi-Qi Xiong[1,2,5*]

Abstract

Chronic methamphetamine (METH) use, a prevalent psychostimulant, is known to impair attention, yet the cellular mechanisms driving these deficits remain poorly understood. Here, we employed a rat model of repeated passive METH injections and evaluated attentional performance using the 5-choice serial reaction time task (5-CSRTT). Using single-nucleus RNA sequencing, immunofluorescence and in situ hybridization, we characterized the response of neurons in the reticulotegmental nucleus (RtTg) to METH exposure. Our results indicate that METH exposure disrupts RtTg neurons at the transcriptional level and results in an increased activation ratio of RtTg under 5-CSRTT conditions. Crucially, chemogenetic inactivation of these neurons or RtTg lesion attenuated METH-induced attention deficits, whereas their activation reproduced the deficits. These findings underscore the critical role of RtTg neurons in mediating METH-induced attention deficits, positioning RtTg as a promising therapeutic target for the treatment of attention deficits linked to chronic METH use.

Keywords Methamphetamine (METH), Attention, Single-nuclei RNA sequencing (snRNA-seq), Reticulotegmental nucleus (RtTg), Five-choice serial reaction time task (5-CSRTT), Designer receptors exclusively activated by designer drugs (DREADD)

Introduction

Methamphetamine (METH), a widely misused psychostimulant, is associated with significant cognitive impairments, particularly affecting attention [1–3]. Chronic METH use impairs attention, marked by difficulties in selectively focusing on stimuli and sustaining attention [4]. However, the precise cellular mechanisms underlying these deficits remain poorly understood.

METH ingestion induces widespread brain stress, altering the function of multiple cell types [5, 6]. Single-nuclei RNA sequencing (snRNA-seq) offers a powerful method to explore transcriptional changes across different neuronal subtypes under identical conditions, providing deeper insights into the cellular dysfunctions associated with METH. For examples, research has identified a subset of glutamatergic neurons as sensitive to cocaine [7], while glial cells have shown sensitivity to both acute morphine and METH exposure [8, 9].

For attention regulation, dopaminergic neurons in the ventral tegmental area impair attention when activated [10], while neurons in locus coeruleus have also been implicated in attention regulation [11]. In addition, pontine nuclei (PN) are a linchpin of the cortico-cerebellar circuit [12, 13], which is activated during the visual attention process [14]. PN have also been reported to be activated during the gaze process in primates [15]. Given the

*Correspondence:
Rongwei Zhai
zhairw@lglab.ac.cn
Zhi-Qi Xiong
xiongzhiqi@ion.ac.cn
[1] Institute of Neuroscience, State Key Laboratory of Neuroscience, CAS Center for Excellence in Brain Science and Intelligence Technology, Shanghai 200031, China
[2] University of Chinese Academy of Sciences, Beijing 100049, China
[3] Shanghai Mental Health Center, Shanghai Jiao Tong University School of Medicine, Shanghai 200031, China
[4] Lin Gang Laboratory, Shanghai 200031, China
[5] Shanghai Center for Brain Science and Brain-Inspired Intelligence Technology, Shanghai 201210, China

role of these neuronal populations in attention regulation, we aim to investigate whether chronic METH exposure alters the transcriptome of neurons in the MB and PN regions, potentially contributing to METH-induced attention deficits.

To explore this, we employed the 5-choice serial reaction time task (5-CSRTT) to assess attentional deficits in a rat model of escalating passive METH injections [16–20]. We then utilized snRNA-seq to identify METH-responsive neurons, which were localized in vivo using immunofluorescence (IF) and in situ hybridization (ISH). Finally, we used the designer receptors exclusively activated by designer drugs (DREADD) system to examine the functional role of these neurons in attention regulation. By integrating behavioral assessments with advanced molecular techniques, this study aims to elucidate the cellular mechanisms underlying METH-induced attention deficits, with a particular focus on the MB and PN.

Materials and methods

Animal ethics and animal feeding

Animal ethics in this paper are by the Institutional Animal Care and Use Committee of the Center for Excellence in Brain Science and Intelligent Technology of the Chinese Academy of Sciences.

Unless indicated otherwise, animals in this paper were subjected to a 12-h light–dark cycle and provided with unrestricted access to both diet and water. The rats obtained from the supplier underwent follow-up testing for a minimum of 2 weeks. Each rearing cage contained three male rats and they were non-aggressive towards each other. Animals were randomly selected for inclusion in the experimental group.

METH injection protocol

The male Sprague–Dawley rats (400–500 g) were subjected to an intraperitoneal injection of 200uL METH saline solution, following a 4-day injection-3-day rest cycle as the published protocol [21, 22]. The METH crystals were gifted from the Anti-Drug Brigade of the Shanghai Public Security Bureau.

Initially, on the first day, the rats received two injections of 0.5 mg/kg each. On the second day, they were given two injections of 1 mg/kg each. On the third day, four injections of 1 mg/kg each were administered. On day 4, the rats were injected four times with a dosage of 1.5 mg/kg. The same injection frequency and dosage were repeated on day 8. On day 9, four injections of 2 mg/kg each were given, followed by four injections of 2.5 mg/kg each on day 10. On day 11, the rats received four injections of 3 mg/kg each. Finally, on day 15 (challenge injection), they were injected four times with a dosage of 4 mg/kg. All injections were administered at 2-h intervals throughout the day.

Single-nuclei sequencing

Single-nuclei sequencing was conducted following the official protocol provided by the 10 × genomic platform. The rats were anesthetized at 72 h after the final injection of METH using sodium pentobarbital at a dosage of 50 mg/kg. Cardiac perfusion was performed using a solution of cold saline. The brain was then extracted and the specific regions of interest were dissected from bregma − 5 to − 9 in a brain module and frozen in liquid nitrogen. Subsequently, the frozen samples were transferred to a temperature of − 80 °C for preservation (< 1 month) and future utilization. For the isolation of single nuclei, the experiment followed the sample preparation guidelines outlined in the "Isolation of Nuclei for Single Cell RNA Sequencing" provided by 10 × Genomic company. The cDNA library was constructed using the 10 × Chromium Single Cell 3′ Reagent Kits (v.2 Chemistry). Sequencing was conducted on the Illumina HiSeq X10 platform, following the manufacturer's instructions. To annotate the raw *. fastq data for subsequent analysis, CellRanger was utilized.

Single-nuclei sequencing data analysis

We used the Seurat R package to analyze the data after obtaining the single nuclei sequencing data from CellRanger. The analysis process began with data normalization, selecting the top 2000 genes with the highest degree of variation for further investigation. A total of 4 samples, 2 treated with METH and 2 treated with Saline, were included in the workflow. The workflow followed the standard approach. For cell type identification and differential gene expression analysis, we utilized the Seurat package following the guidelines provided by Satijalab. To gain insights into the biological functions, KEGG and Gene Ontology analysis were applied using the KOBAS website [23], utilizing the feature gene list of Transcriptomic cluster-15.

Immunofluorescent

The process began with euthanizing the rats using carbon dioxide and the brain was collected 3-day post METH or saline challenge injection. The brain was then extracted without perfusion [24] and submerged in a 4% PFA-PBS (PBS: 137 mM NaCl, 2.7 mM KCl, 10 mM $Na_2HPO_4{\cdot}2H_2O$, 2 mM KH_2PO_4, pH 7.4) solution. Subsequently, it was stored overnight at 4 °C. The brain tissues underwent gradient dehydration using 15% and 30% sucrose-PBS solutions at 4 °C. Following this, the brains were sectioned into desired blocks using brain molds and embedded in OCT (Sakura 4583) compound.

For the coronal brain sections, the RTTG brain region was sampled at a thickness of 25 μm using a 1:8 ratio (i.e. for 25 μm brain slices, we collected one slice every 200 μm). For the sagittal brain sections, the brain sample was collected at a thickness of 40 μm. A blocking buffer was prepared with 0.1% triton-X, 5% BSA in 1×TBS (20 mM Tris, 0.137 M NaCl, pH7.6) The brain sections were incubated in the blocking buffer at room temperature for 30 min with shaking. Then, the primary antibody was added and the sections were further incubated at 4 °C for 24 h. After two washes with wash buffer (0.1% Tween20 in 1×TBS), the secondary antibody was introduced and incubated at room temperature for 1.5 h with continuous shaking. All antibodies were diluted in a blocking buffer. Subsequently, the sections were positioned on top of 1×TBS in a sterile cell culture dish, mounted onto glass slides, and sealed with nail polish after surplus moisture evaporation. The mounting medium containing DAPI (Beyotime P0131) was applied for nuclear staining.

The primary antibodies used in this experiment and their dilutions were as follows: NFIB (Abcam ab186738) 1:2000, NeuN (Abcam ab104224) 1:2000, CaMKII (Abcam 181052) 1:2000, Gad1/2 (Abcam 183999) 1:2000 and c-fos (Abcam ab190289) at a 1:2000. As for the secondary antibodies, they were Donkey anti-Mouse Alexa Fluor Plus 488 (Thermofisher A32766) diluted at 1:1000 and Donkey anti-Rabbit Alexa Fluor Plus 647 (Thermofisher A31573) diluted at 1:2000.

The sections were then screened using the Olympus VS120 and analyzed with ImageJ software [25]. Integrated intensity from multiple brain slices containing the RtTg (or BPN) region was obtained for each rat and divided by the total area (measured in ImageJ) to calculate the mean intensity per sample. These mean intensities were subsequently normalized by dividing each by the average mean intensity of RtTg from saline-treated rats, yielding the relative fold change. For c-fos quantification, ImageJ's "Analyze Particles" feature was used to count c-fos and NeuN-positive cells.

In situ hybridization

In order to perform in situ hybridization, the brain sections were first affixed onto slides and then subjected to staining, following the manufacturer's instructions of ACD's RNAscope™ 2.5 HD Duplex Assay (332430) or RNAscope™ Multiplex Fluorescent Reagent Kit (323100). Frozen brain sections were cut into 15 μm and collected at a 1:10 ratio then mounted onto glass slices for the following test. The probes used are RNAscope™ Probe-Rn-*Hapln2* (588221) diluted at 1:2 and RNAscope™ Probe-Rn-*Slc17a7*-C2 (317001-C2) diluted at 1:100. The diluent used is RNAscope™ Probe Diluent (300041). For the fluorescent ISH, the probe utilized was RNAscope™ Probe-Rn-*Slc17a6* (317011), RNAscope™ Probe-Rn-*Slc32a1* (424541), the RNAscope™ Probe-Rn-*Slc17a7*-C2 and RNAscope™ Probe- Rn-*Fos*-C3 (430591-C3) was diluted in accordance with the manufacturer's instructions. The sections were then screened using the Olympus VS120 and analyzed with ImageJ software as the IF step.

RNA–protein in situ co-detection

The Integrated Co-Detection workflow (ICW) was performed in accordance with the official guidance of RNA–Protein Co-detection kit (RNAscope™ 323180). The combination of the RNA ISH kit and Probe was previously described in the ISH procedure. In the ICW, the NFIB antibody dilution was 1:500 and the Donkey anti-Rabbit Alexa Fluor Plus 647 was 1:1000.

The NFIB antibody was diluted in Co-detection Antibody Diluent and incubated in 4 °C overnight. The secondary antibody was diluted in Co-detection Antibody Diluent and incubated at room temperature for 1 h.

Stereotactic surgery

According to the study conducted by Ali Cetin et al. [26], stereotactic surgery was performed. Anesthesia was administered to the rats using a 2% isoflurane solution, which was then sustained at a concentration of 1% using a stereotaxic apparatus. The injection site for AAV injection was determined based on Bregma coordinates. For RtTg injection, the chosen site was (ML: 0, AP: −8.5, DV: −10.5). A control injection sites were used at (ML: 0, AP: −8.5, DV: −7) in Fig. 4E. The AAV activity was diluted to a concentration of 2E+12 viral genomes per microliter (V.E./mL), and a total volume of 300 nanoliters (nL) was used.

The AAV was provided by Shanghai Taitool Bioscience Co., Ltd. The catalog of the used AAV in our experiment was:

AAV2/9-mCaMKIIa-hM4D(Gi)-mCherry-ER2-WPRE-pA: S0494.

AAV2/9-mCaMKIIa-hM3D(Gq)-mCherry-ER2-WPRE-pA: S0484.

AAV2/9-mCaMKIIa-mCherry-WPRE-pA: S0242.

For the RTTG lesion, the injection sites for Kainic Acid and PBS were randomly assigned to (ML: 0.5, AP: −8.5, DV: −10.5) or (ML: −0.5, AP: −8.5, DV: −10.5). Kainic Acid (MCE HY-N2309), at a concentration of 1 mg/ml in a 1×PBS solution, was injected at a volume of 250nL. For the Sham surgery group, 250nL of 1×PBS was injected.

The injection was performed using glass microelectrodes. After the injection, it was standard practice to leave the needle in place for 5 min before removing it. Following hemostasis, disinfection, and suturing procedures,

the subject was placed in a cage to recover naturally. No experimental procedures were conducted within 2 weeks after the surgery. Each rat was housed in an individual cage with access to ad libitum food and water. After a 2-week recovery, the rats gradually reintroduced the practice of the 5-CSRTT. This behavior resorting process continued 1 week and then discard the rats unable to restore their 5-CSRTT performance.

5-Choice serial reaction time task

The 5-choice serial reaction time task (5-CSRTT) is conducted as published protocol [17, 27]. Given that attentional impairment has been observed in rodents following METH administration, our 5-CSRTT is a simplified version with a 2-s stimulation duration [18, 27–33]. In our test, a food and water-restricted rat is placed in the 5-CSRTT apparatus, where one of five poke lights is illuminated 5 s after the rat triggers the food tray, and the rats are rewarded for correctly touching the illuminated light in the next 5 s (Fig. S1A, B). The 5-CSRTT was performed between 11:00 AM and 11:00 PM.

The training process involves gradually shortening the poke lights' duration. In this experiment, the gradient configuration includes time intervals of 30 s, 10 s, 5 s, 3 s, and 2 s. After achieving stable performance in the 2-s 5-CSRTT task, rats may proceed to subsequent experiments if their average Omission% was below 30% for three consecutive days. Following each training session, rats have 1 h of free access to food and water. The reward employed in the 5-CSRTT task consists of a single droplet of sucrose solution with a concentration of 20%.

In the data collection step, rats enter the behavior training box at similar times daily and perform a 30-min 5-CSRTT test, with data automatically recorded by the software provided by Anilab (AES-130). To ensure consistency, all experimental groups were evenly distributed across the time slots through a cross-arrangement. The rats were also food and water restricted and rats have 1 h of free access to food and water after they complete daily task. The software records the Correct action, Error action, Omission action, and Premature action. The calculation method for Correct%, Omission%, and Premature% as follows:

$$\text{Correct\%} = \text{Correct actions}/(\text{Correct actions} + \text{Error actions}) * 100\%$$

$$\text{Omission\%} = \text{Omission actions}/(\text{Correct actions} + \text{Error actions} + \text{Omission actions}) * 100\%$$

$$\text{Premature\%} = \text{Premature actions}/(\text{Correct actions} + \text{Error actions} + \text{Omission actions} + \text{Premature actions}) * 100\%.$$

For rats that have received AAV injections for neuronal activation, a 10 μg/ml deschloroclozapine (abbreviation: DCZ, catalog: MCE HY42110) solution is administered intraperitoneally at a dosage of 4 μg/kg, 40 min before the behavioral experiment begins. For the purpose of inhibiting neuronal activity and prevent RtTg activation in subsequent c-fos staining, we prolonged the inactivation duration by the DCZ was i.p. inject-ed at a dosage of 4 μg/kg, 2 h and 40 min prior to the 5-CSRTT and an additional DCZ injection is administered 1d prior to the first day to balance the subsequent daily DCZ intake.

The compound DCZ is initially dissolved in dimethyl sulfoxide (DMSO) at a concentration of 10 mg/ml and then combined with saline in a ratio of 1:1000. The control Vehicle (Veh) is a 0.1% DMSO-Saline solution.

The data was collected in 2–4 continuous days in the 5-CSRTT experiment without METH administration. The injection schedule for DCZ or Veh was as presented in the previous figure. The data presented in Fig. 3C, G were collected over the course of two consecutive days (1-day and 2-day post-weekly METH injection, respectively) and subsequently averaged for analysis. Challenge 5-CSRTT is provided in the 3-day and 4-day post-METH challenge injection. On the 1st and 2nd-day post-METH challenge injection, the rat undergoes a 2-s pokelight duration 5-CSRTT test. On the 3rd day, the pokelight duration is 1 s. On the 4th day, the pokelight duration is 3 s.

Shuttle test

The Shuttle test was post-completion of the 5-CSRTT test. The content of the Shuttle test involves the utilization of the behavior paradigm previously described, wherein all five pokelights are illuminated simultaneously and remain lit until they are triggered. Touching any pokelight at any given moment will yield a reward (Fig. S5B). If the data remains stable, the test proceeds to the data collection phase. This experiment is also conducted under food restriction, and rats are provided with 1 h of free feeding time after completing their daily tasks. The data is automatically collected by the 5-CSRTT software as previously mentioned. The DCZ or Veh injection

protocol was as the previous 5-CSRTT described. The data were collected over the course of three consecutive days, after which the mean values were calculated for subsequent analysis.

Progressive ratio test

The Progressive ratio test, which is based on the fundamental principle that rats receive food as a result of repeated activation of the Foodtray, determines the ratio between the number of times the rat triggers the Foodtray and the reward it receives. The ratio is determined based on the reward amount, with a ratio of 1 for rewards between 0 and 20, a ratio of 2 for rewards between 20 and 30, a ratio of 5 for rewards between 30 and 35, and a ratio of (5*e^0.2(Reward-35) − 1) for rewards greater than 35.

For rats injected with METH, the Reward Desire test is conducted on the same day as the 5-CSRTT tests. The rats in the METH injection and 5-CSRTT group differ from the rats in the METH injection and Reward Desire test group. Both groups of rats are exposed to the same experimental conditions in terms of the 5-CSRTT testing environment and the environment for administering METH injections.

Data analysis

For all behavioral and optical microscopy data in this experiment, we employed ANOVA or 2-way ANOVA analysis. Subsequently, statistical corrections were applied using methods such as Bonferroni. In the case of a comparison between two groups, t-tests were utilized. All calculations were performed using GraphPad Prism 9.0.0. All error bars in this study are presented as SEM (standard error of the mean).

The optical density of the imaging data was measured using ImageJ, and the normalized integrated optical density was calculated by dividing it by the average value of the control group's integrated optical density.

For the analysis of single-nuclei sequencing data, we followed the methods implemented in the Seurat [34].

Results

Chronic METH intake induces attention deficit in rats

The escalating dose METH injection protocol is a well-established method used to mimic the clinical patterns of METH use, where doses begin low and progressively increase [22]. This protocol frequently employed to study METH-related behavioral abnormalities or their molecular underpinnings [35–38]. Rats received 9 days of intraperitoneal (i.p.) METH injections over a 15-day period. METH was administered 4 days per week, followed by assessment using the 5-CSRTT on days five through seven (Fig. 1A).

A significant increase in Omission%, an indicator of attention where higher values denote reduced attention, was observed in METH-treated rats compared to the saline control group ($p < 0.001$, post challenge day 3, Fig. 1B; see Supplement Data 1 for detailed statistics). This elevated Omission% persisted from 1 to 4 days following the cessation of METH injections. In contrast, Correct%, another measure of attention, did not differ significantly between the METH and control groups after 2 days. Furthermore, impulsivity, as measured by Premature%, was not affected by METH treatment (Fig. 1B).

Since the 5-CSRTT relies on reward-driven behavior (with sucrose as the reward), we evaluated whether METH affected these animals' motivation for sucrose using a progressive ratio (PR) task. To ensure consistent experimental conditions, including METH administration and fasting, we used the same setup as the 5-CSRTT. Compared with food restriction (-Food), we used ad libitum feeding (+Food) as a positive control, we confirmed that our PR protocol can detect decreases in motivation ($p = 0.004$, Fig. S1C). The results indicated that METH did not diminish the motivation for sucrose required for 5-CSRTT performance ($p = 0.999$ METH vs. Saline, post-challenge day 2, Fig. 1C). Overall, these findings suggest that the METH treatment protocol effectively induces attention deficits without significantly affecting other measured components within our experimental framework.

RtTg neurons exhibit cell-type-specific responses to METH

Because the Omission% in METH-treated rats increased steadily from the second to the fourth day and the Correct% remained indifferent compared to the Saline group during this period, brain tissue samples from the MB and PN regions (referred to as MB plus tissue, Bregma: − 5 to − 9) were collected on the third day after the final METH injection (Fig. 2A). Using the commercial 10 × genomic drop-seq-based snRNA-seq library

(See figure on next page.)

Fig. 1 Chronic METH use induces attention deficit. **A** Schematic representation of the METH injection and 5-CSRTT schedule, with dosages ranging from 0.5 to 4 mg/kg per injection. **B** Results of the 5-CSRTT in rats after METH or saline treatment (Saline, n = 12; METH, n = 13, $^{*}p < 0.05$; $^{**}p < 0.01$; $^{***}p < 0.001$, 2-way ANOVA with Bonferroni correction, Saline vs. METH). **C** Progressive ratio test outcomes after METH or saline treatment, with identical environmental settings as the 5-CSRTT (Saline, n = 10; METH, n = 12, 2-way ANOVA with Bonferroni correction, Saline vs. METH, all $p > 0.05$; Reward intake change = (Reward intake − Reward intake$_{Pre\text{-}average}$)/Reward intake$_{Pre\text{-}average}$)

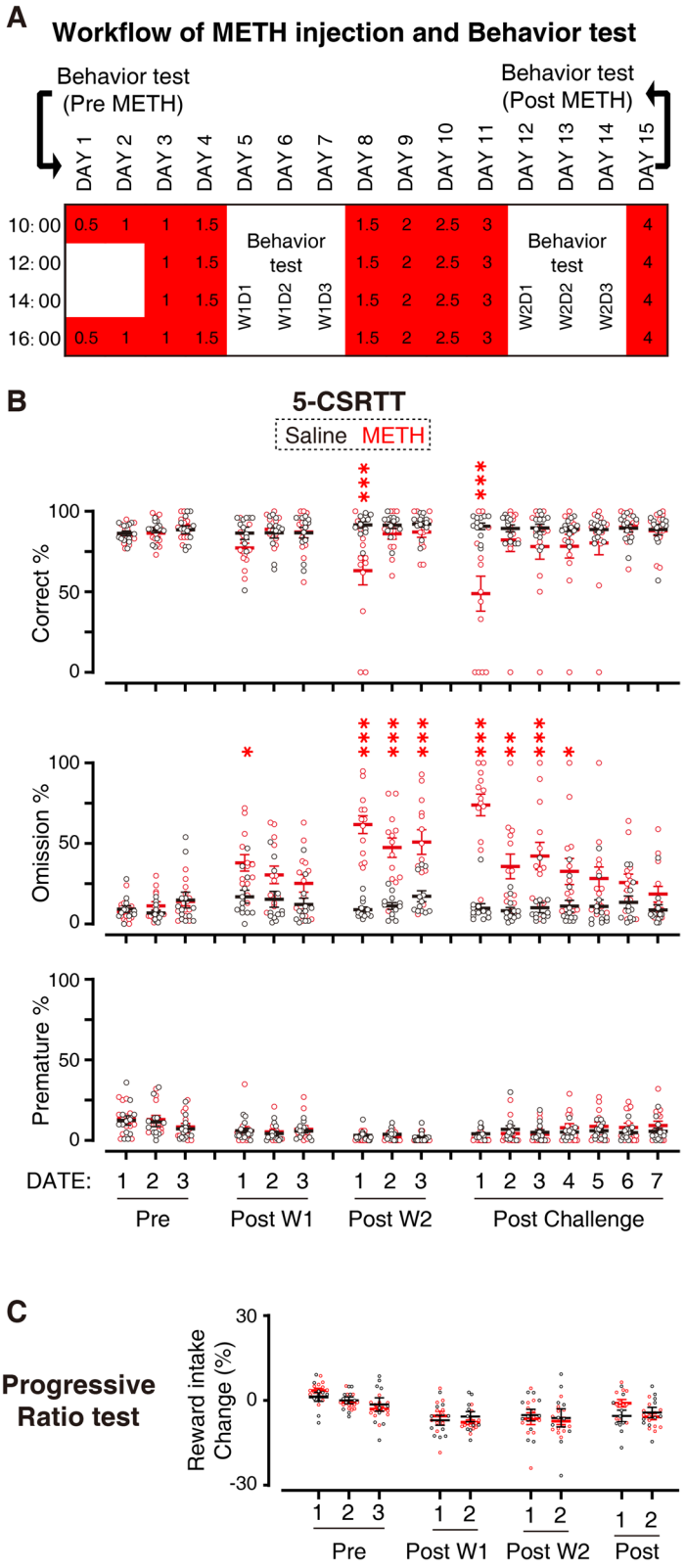

Fig. 1 (See legend on previous page.)

construction system and Seurat for data analysis [34], we identified 24 distinct cellular transcriptomic clusters (TCs) within the MB plus tissue through anchor-based reciprocal PCA integration of the sequence data. Notably, a neuronal TC labeled TC-15, characterized by the highly expressed pan-neuron marker *Syt1*, was significantly increased following METH exposure (Fig. 2B). This TC also displayed elevated expression of *Slc17a7*, which encodes the vesicular glutamate transporter 1 (VGLUT1), a classic marker of glutamatergic neurons [39]. In contrast, other neuronal markers, such as *Slc17a6* (VGLUT2 glutamatergic neurons), *Slc32a1* (GABAergic neurons), and *Th* (dopaminergic neurons), showed low expression in TC-15, confirming that this cell TC is a VGLUT1-positive glutamatergic neuron (Figs. 2C and S2A).

To determine the in vivo localization of TC-15, we utilized IF staining to detect the top-ranked feature genes, including *Nfib* and *Slc17a7*. Based on both IF data and public databases, we found that no other nuclei in this brain region exhibited high levels of Nuclear Factor I/B (NFIB) protein except for PN (Fig. 2D). PN primarily contains reticulotegmental nucleus (RtTg) and basilar pontine nucleus (BPN). IF staining showed that NFIB expression was higher in RtTg compared to BPN (RtTg vs. BPN: $p=0.023$ in Saline group, $p=0.001$ in METH group, Fig. 2E, G). NFIB protein levels were also significantly elevated in RtTg after METH exposure ($p=0.004$, Fig. 2E, G), while NeuN levels remained unchanged ($p=0.087$). Additionally, RNA in situ hybridization (ISH) confirmed these findings, showing increased *Slc17a7* expression ($p=0.001$) in RtTg following METH exposure, whereas *Hapln2* expression remained stable ($p>0.999$ Fig. 2F, G). These results align with the observed increase in TC-15 cells after METH treatment.

Next, IF staining of NeuN and NFIB confirmed that the RtTg neurons are NFIB + (Fig. 2H). Consistent with previous findings [40–43], our IF staining further demonstrated that RtTg neurons are glutamatergic, as evidenced by co-localization with the neuronal marker NeuN and the glutamatergic marker CaMKII (Fig. 2I). Moreover, we investigate whether the *Slc17a7*-positive neurons were also NFIB-positive. Using RNA–protein co-detection assays, we validated that the *Slc17a7*-positive neurons were NFIB-positive (Fig. S2B). Additionally, RNA ISH data confirmed that RtTg neurons are negative for *Slc17a6* and *Slc32a1*, which is consistent with the snRNA-Seq results (Fig S2C). Taken together, these co-localization studies confirmed that RtTg neurons are glutamatergic and correspond to cell TC-15 identified by snRNA-Seq.

Inactivation of RtTg neurons reverses METH-induced attention deficits

To investigate whether the activity of RtTg neurons contributes to METH-induced attention deficits, we utilized the DREADD system to selectively inactivate these neurons (Fig. 3A for workflow). Since RtTg neurons are glutamatergic and express CaMKII, we employed an AAV-mediated DREADD system, specifically using AAV2/9-mCaMKIIa-hM4Di-mCherry-WPRE-ER2-pA (hM4Di) or AAV2/9-mCaMKIIa-mCherry-WPRE-pA (mCherry) to target RtTg neurons (Fig. 3B). Rats were divided into two experimental groups: one receiving AAV-hM4Di and the other receiving AAV-mCherry. Both groups were injected with METH and subjected to the 5-CSRTT, forming the METH + hM4Di and METH + mCherry groups, respectively. As a control, a third group of rats infected with AAV-mCherry received saline injections (Saline + mCherry group). To specifically inhibit hM4Di-infected neurons without affecting mCherry-infected neurons, we administered Deschloroclozapine (DCZ) via i.p. injection after METH challenge injection. During the first and second weeks of the 5-CSRTT experiment, DCZ was withheld to allow the METH-induced attention deficits to manifest.

(See figure on next page.)

Fig. 2 RtTg neurons exhibit cell type-specific responses to METH. **A** Rat brains were collected on day 3 post-METH exposure, brain tissues (labeled blue) containing midbrain (MB) and pontine nuclei (PN) were collected for subsequent single nuclei sequencing. **B** Uniform manifold approximation and projection (UMAP) of the tissue sample single nuclei sequencing results showed an increase in Cell Transcriptomic cluster (TC) – 15 following METH exposure. **C** Selected feature genes of MB samples. *Slc17a7 and Nfib* were identified as feature genes of TC-15 by Seurat (Classical cell subtype markers: *Syt1*: Pan-neuron marker, *Hapln2:* Oligodendrocyte, *Slc17a7*: VGLUT1 + glutamatergic neuron marker, *Slc17a6*: VGLUT2 + glutamatergic neuron marker, *Slc32a1*: GABAergic neuron marker). **D** Immunofluorescence (IF) of TC-15 marker NFIB in METH treated rats, PN expressed a higher level of cellular NFIB and PN mainly divided into RtTg and BPN. The color was inverted. **E** Immunofluorescence (IF) of TC-15 marker NFIB, with NeuN as control. RtTg and BPN are two of the major nucleuses of PN. RtTg cellular NFIB was higher than BPN and METH exposure caused NFIB increase in RtTg. **F** In situ hybridization (ISH) of TC-15 marker *Slc17a7*, with *Hapln2* as quality control. **G** Relative NFIB (n = 10) and NeuN (n = 8) protein expression levels in RtTg and BPN (**$p<0.01$; *$p<0.05$; ns $p>0.05$; 2-way ANOVA with Bonferroni's multiple comparison test). Relative *Slc17a7* and *Hapln2* RNA expression levels in RtTg and BPN (Saline, n = 6; METH, n = 8; **$p<0.01$, Bonferroni's multiple comparison test). **H** IF of NFIB and mature neuron marker NeuN in METH treated rats. In RtTg, neurons are NFIB positive. **I** IF of NeuN and glutamatergic neuron marker CaMKII in METH treated rats, RtTg neurons are glutamatergic neurons

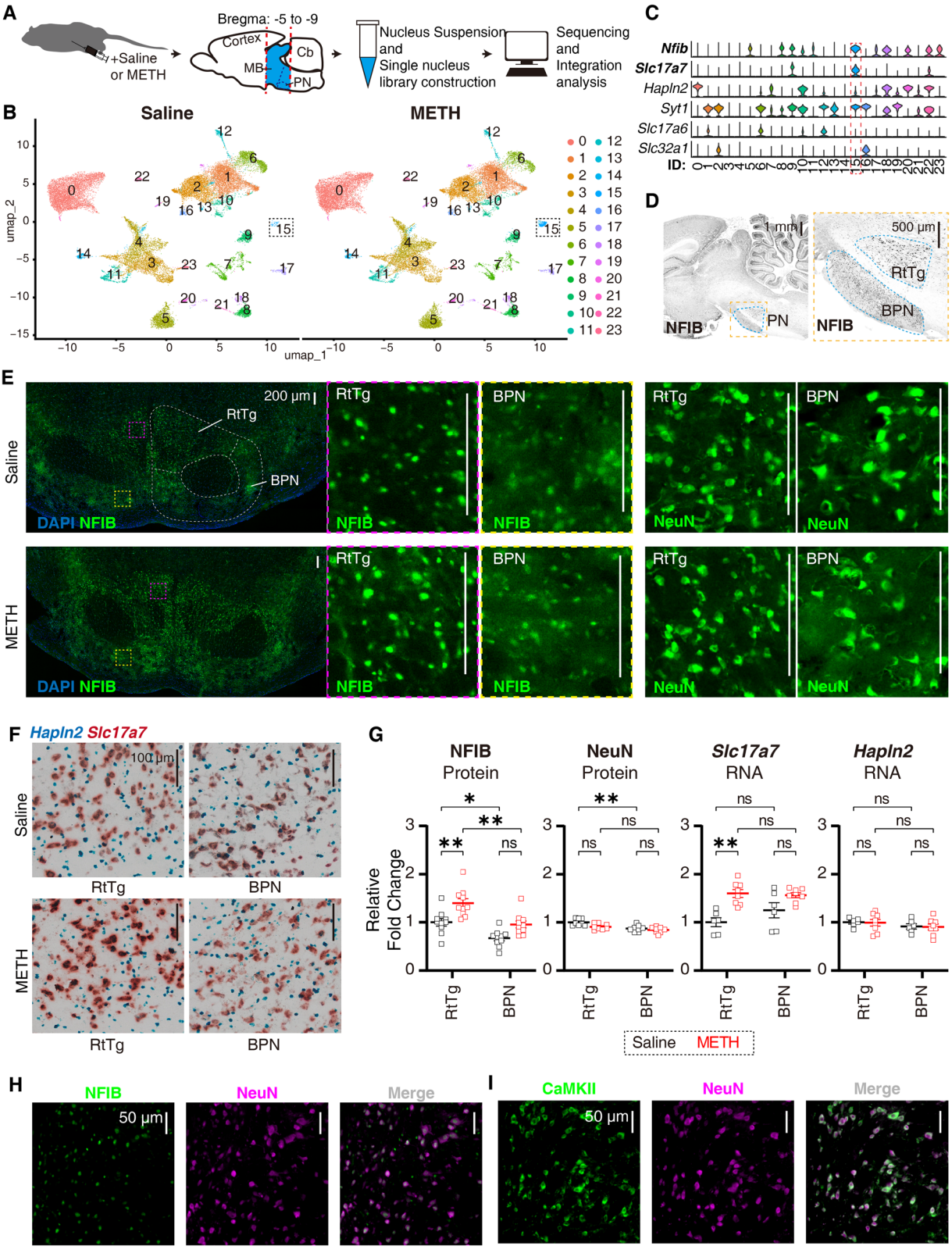

Fig. 2 (See legend on previous page.)

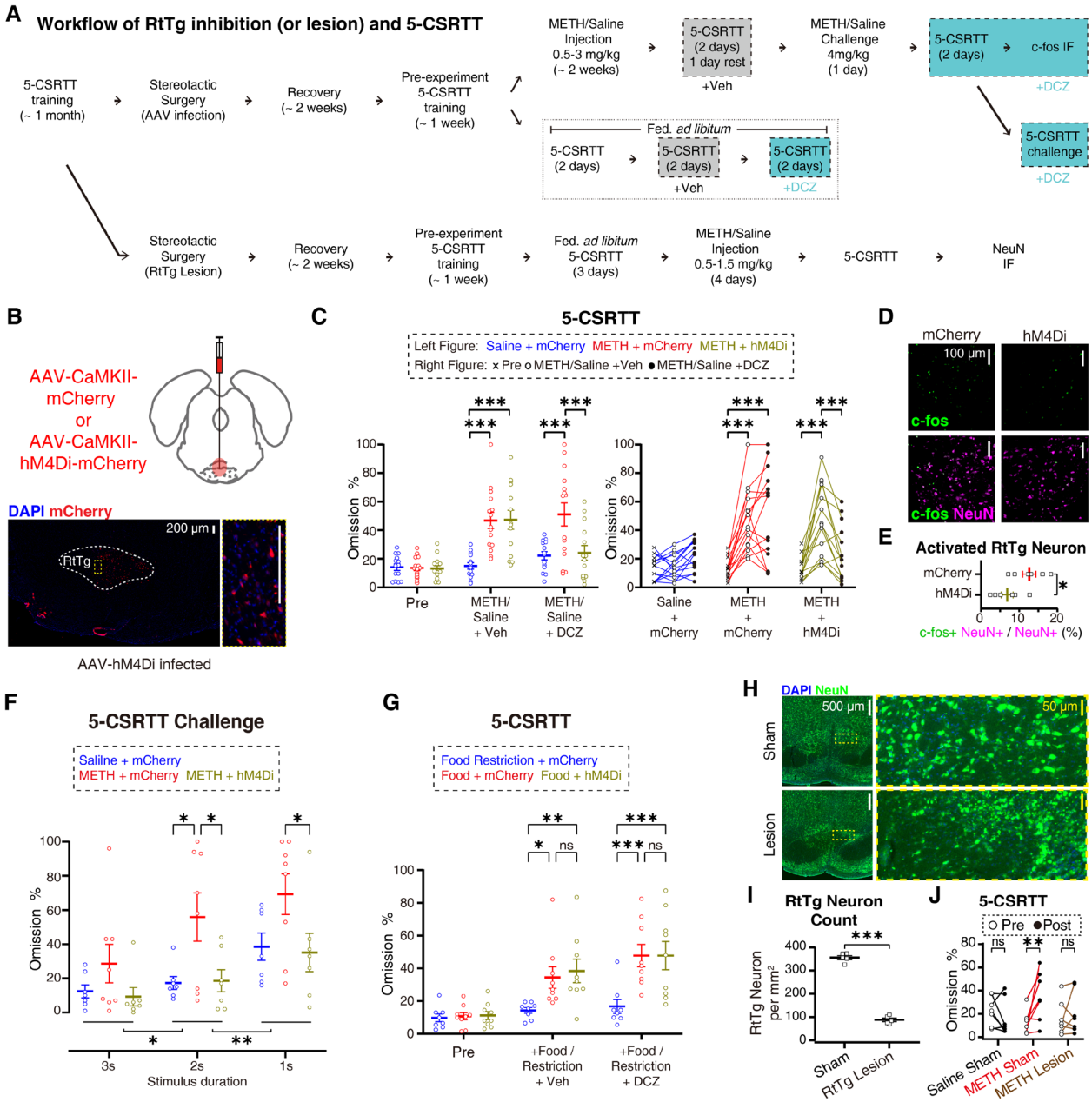

Fig. 3 Inactivation of RtTg neurons reverses METH-induced attention deficits. **A** Workflow of chemogenetic RtTg suppression or RtTg lesion, METH treatment and 5-CSRTT. **B** Top: Schematic of the AAV injection site for AAV2/9-mCaMKIIa-mCherry-WPRE-pA (mCherry) or AAV2/9-mCamkIIa-hM4Di-mCherry-WPRE-ER2-pA (hM4Di). Bottom: Expression of hM4Di-mCherry in RtTg. **C** 5-CSRTT performance of AAV-infected rats following METH exposure. RtTg neurons were inhibited in the AAV-hM4Di-infected rats after DCZ i.p. injection. The METH-induced increase in Omission% was confirmed in AAV-mCherry-infected rats. The right panel shows paired Omission% data from the left panel (Saline + mCherry, n = 14; METH + mCherry, n = 15, METH + hM4Di, n = 14; ***p < 0.001, 2-way ANOVA with Bonferroni correction). **D** IF staining for c-fos and NeuN in RtTg after the final 5-CSRTT test. Samples were collected after METH and DCZ administration as shown in (**C**). **E** Statistics of RtTg neuron activation ratio (n = 6 both groups; *$p < 0.05$, unpaired *t*-test). **F** 5-CSRTT challenge test following METH exposure, with increased attention demands by reducing pokelight stimulus duration (Saline + mCherry: n = 7; METH + mCherry: n = 8; METH + hM4Di: n = 7; *$p < 0.05$, 2-way ANOVA with Bonferroni correction). **G** Effect of RtTg neuron inhibition on additional food-induced increase in Omission% (Food restriction + mCherry, n = 8, Food + mCherry, n = 9, Food + hM4Di, n = 9; *$p < 0.05$; **$p < 0.01$; ***$p < 0.001$; ns, $p > 0.05$, 2-way ANOVA with Bonferroni correction). **H** IF staining of the mature neuron marker NeuN in the kainic acid-mediated RtTg lesion group, with PBS injection as sham surgery control. **I** Statistics of RtTg neuron number after RtTg lesion (n = 5 for both groups; ***$p < 0.001$, unpaired *t*-test). **J** 5-CSRTT performance of the RtTg-lesioned rats following METH exposure (n = 7 per group; **$p < 0.01$; ns, $p > 0.05$, 2-way ANOVA with Bonferroni correction)

Compared to the Saline + mCherry group, both METH-treated groups (METH + hM4Di and METH + mCherry) exhibited the significant increases in Omission% (both $p < 0.001$), confirming the attention impairments induced by METH. Following the METH challenge injection, DCZ was administered to all groups. Notably, the Omission% in the METH + hM4Di group decreased significantly compared to the METH + mCherry group ($p < 0.001$), returning to levels similar to the control Saline + mCherry group ($p > 0.999$, Fig. 3C). Additionally, a comparison of the Omission% values before and after DCZ treatment revealed that DCZ significantly reduced Omission% in the METH + hM4Di group ($p < 0.001$) but had no effect in the METH + mCherry group ($p = 0.983$, Fig. 3C). This was further corroborated by c-fos staining of RtTg neurons, which showed reduced activation in the METH + hM4Di group compared to the METH + mCherry group ($p = 0.032$, Fig. 3D, E).

To ensure that the increased Omission% accurately reflected attention deficits rather than stereotyped behavior or cognitive decline from repetitive 5-CSRTT testing, we adjusted task difficulty by manipulating the stimulus duration. In subsequent tests, we conducted a 5-CSRTT challenge test after the METH challenge injection, confirming that Omission% increased as pokelight duration decreased ($p = 0.003$, 2 s vs. 1 s). Under the 1 s pokelight duration, post-DCZ injection, rats in the METH + hM4Di group showed Omission% values similar to the Saline + mCherry group ($p > 0.999$), and was significantly lower than the METH + mCherry group ($p = 0.046$, Fig. 3F).

To confirm the specificity of RtTg inhibition in reversing METH-induced attention deficits, we examined the effects of conditions unrelated to RtTg neuron activation, such as food intake. Since RtTg neurons are not activated by food consumption [44], we assessed whether ad libitum feeding, which typically increases Omission%, influenced attention. In the + Food condition, rats fed ad *libitum* had significantly higher Omission% compared to those under food restriction (+ Food + mCherry vs. Food restriction + mCherry, $p = 0.037$). Notably, this increase persisted following DCZ injection in both the hM4Di and mCherry groups (+ Food + hM4Di vs. + Food + mCherry, $p > 0.999$, Fig. 3G), confirming that RtTg inhibition specifically reversed METH-induced attention deficits without affecting food-related behavior.

The RtTg lesion was used as a technical validation of DREADD-mediated inhibition. Stereotactic injection of kainic acid induced RtTg lesions, with PBS injection as a sham control [45]. NeuN IF staining confirmed significant neuronal loss in the RtTg-lesioned rats (Fig. 3H, I). Following the RtTg lesions, rats were treated with METH for 4 days and subjected to the 5-CSRTT for 1 day. The Omission% in the RtTg-lesioned rats did not increase under METH treatment (Fig. 3L). Omission% values in the METH + RtTg lesion group after METH injection were similar to the METH + RtTg group pre-METH treating ($p = 0.202$). However, under same METH injection condition, the Omission% in METH + Sham group was significantly increased ($p = 0.008$, Fig. 3L). The Omission% increase level ($\text{Omission\%}_{\text{Post}}$- $\text{Omission\%}_{\text{Pre}}$) in METH + RtTg group was significantly lower than METH + Sharm group ($p = 0.009$, Fig. S3B). Consistent with the RtTg inhibition results, RtTg lesion did not affect food-induced increases in Omission% ($p = 0.689$, Fig. S3C right). Together, these results suggest that METH is unable to impair attention in the absence of functional RtTg neurons.

Chronic METH intake increases activation ratio of RtTg neurons

We then investigated the functional implications of the METH-induced effects on RtTg neurons. Since the increase in TC-15 cells was linked to the upregulation of RtTg feature genes, we performed KEGG and GO analyses to evaluate the functions of these genes [23]. The analyses revealed an enrichment of glutamate synapse-related genes (Fig. 4A), including *Grik1* and *Grm8* genes, which are involved in prevention of excitotoxicity [46, 47] (Fig. 4B, Supplement Data 2). These findings prompted us to investigate whether the METH-treated RtTg neurons were prone to activation.

To assess this, we collected rat brains after METH or saline injections combined with the 5-CSRTT test. Brains were harvested on the second day post-METH challenge, 30 min post 5-CSRTT. IF staining for c-Fos showed increased activation of RtTg neurons after METH exposure ($p = 0.033$, Fig. 4C, D). Since RtTg was analyzed 48 h after the last METH injection, it is unlikely that the activation was directly caused by acute METH effects. This was supported by snRNA-Seq data, RtTg fos gene positive cells were rare in cell TC 15 (Fig. S4A) and activated RtTg neurons were rare in 5-CSRTT untrained rats (Fig. S4B).

Activation of RtTg neurons reproduces METH-like attention deficits

To determine whether activation of RtTg neurons alone could reproduce METH-like attention deficits in rats that had not been exposed to METH, we utilized the DREADD system to activated these neurons (Fig. 5A). Since RtTg neurons are glutamatergic, we stereotactically injected the hM3Dq gene via adeno-associated virus (AAV2/9-mCaMKIIa-hM3Dq-mCherry-WPRE-ER2-pA) into the RtTg, followed by i.p. injection of DCZ to selectively activate the hM3Dq-infected neurons. As a control,

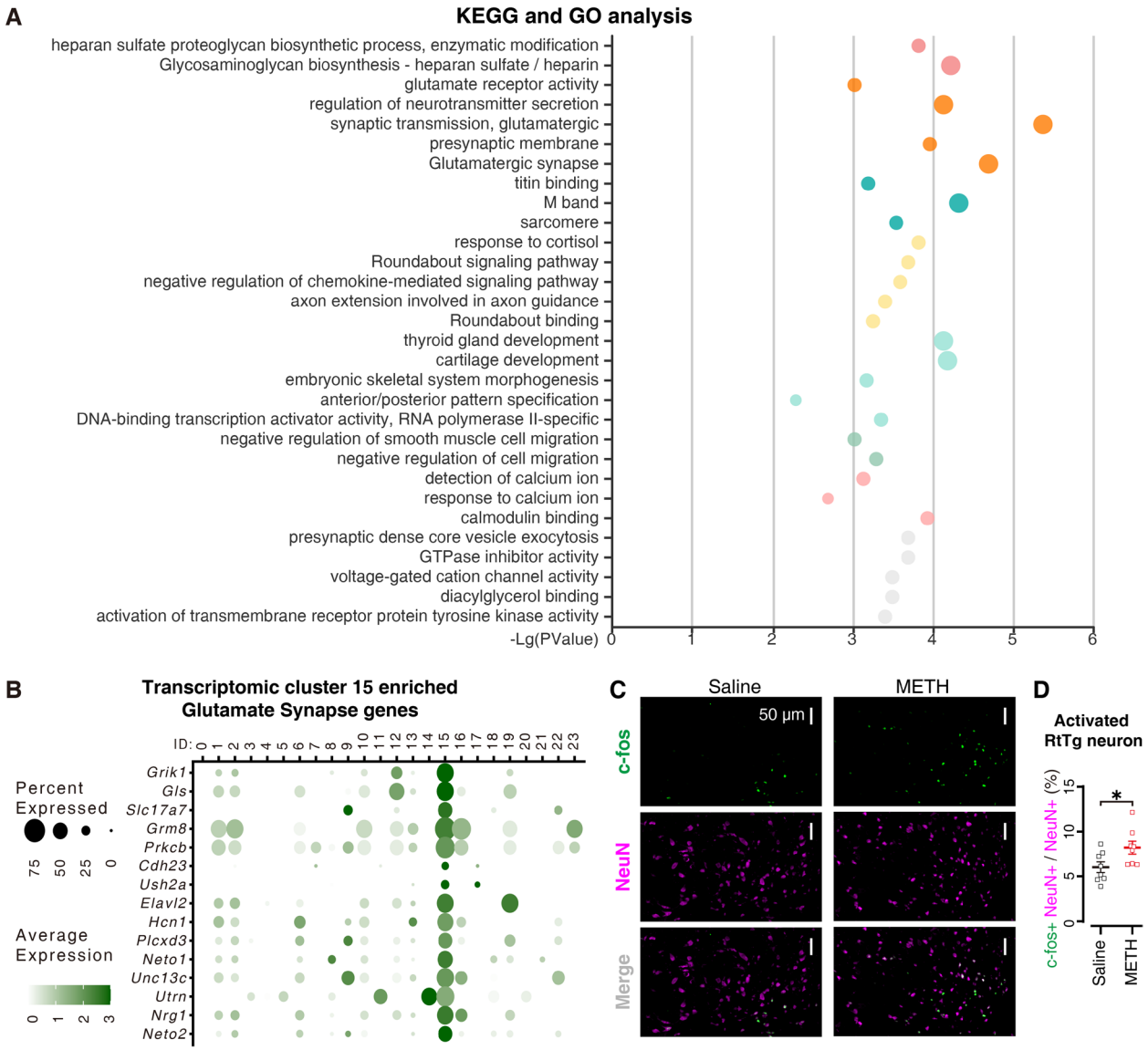

Fig. 4 Chronic METH intake increases activation ratio of RtTg neurons. **A** KEGG and GO analysis revealed alterations in the expression of genes associated with glutamate synapses in RtTg neurons. The differentially expressed genes were identified using the top 100 feature genes of TC-15. The number of genes within a given pathway is directly proportional to the size of the bubble displayed on the bubble map. Different colors are used to represent different clusters. **B** Genes related to glutamatergic synapses that are enriched in METH-responsive cell TC 15. **C** Expression of neuron activation marker c-fos in RtTg and NeuN was co-localization neuron marker. **D** Statistics of RtTg neuron activation ratio after METH exposure (n = 8 per group, $^{*}p < 0.05$, unpaired *t*-test)

the ventral tegmental nucleus (VTg) was also infected, along with control AAV injection (AAV-mCherry or AAV-hM4Di) into RtTg (Fig. 5B, C). The activation of RtTg neurons was confirmed by increased expression of the activity marker c-fos ($p < 0.001$, Fig. 5D).

In the 5-CSRTT, after DCZ-induced activation of RtTg neurons, there were no significant changes in Correct% ($p = 0.410$) and Premature% ($p = 0.580$). However, Omission% in the RtTg hM3Dq-infected group significantly increased after DCZ (4 μg/kg) injection ($p = 0.001$, Fig. 5E), whereas Omission% in the VTg hM3Dq-infected group remained unchanged ($p > 0.999$, Fig. 5E). In a separate 5-CSRTT test, where we reduced the DCZ dose to 1 μg/kg, the hM3Dq-infected group still exhibited a significant increase in Omission% after DCZ injection ($p = 0.002$, Fig. 5F). Both the mCherry and hM4Di control groups showed no significant changes in Omission% after DCZ injection (both

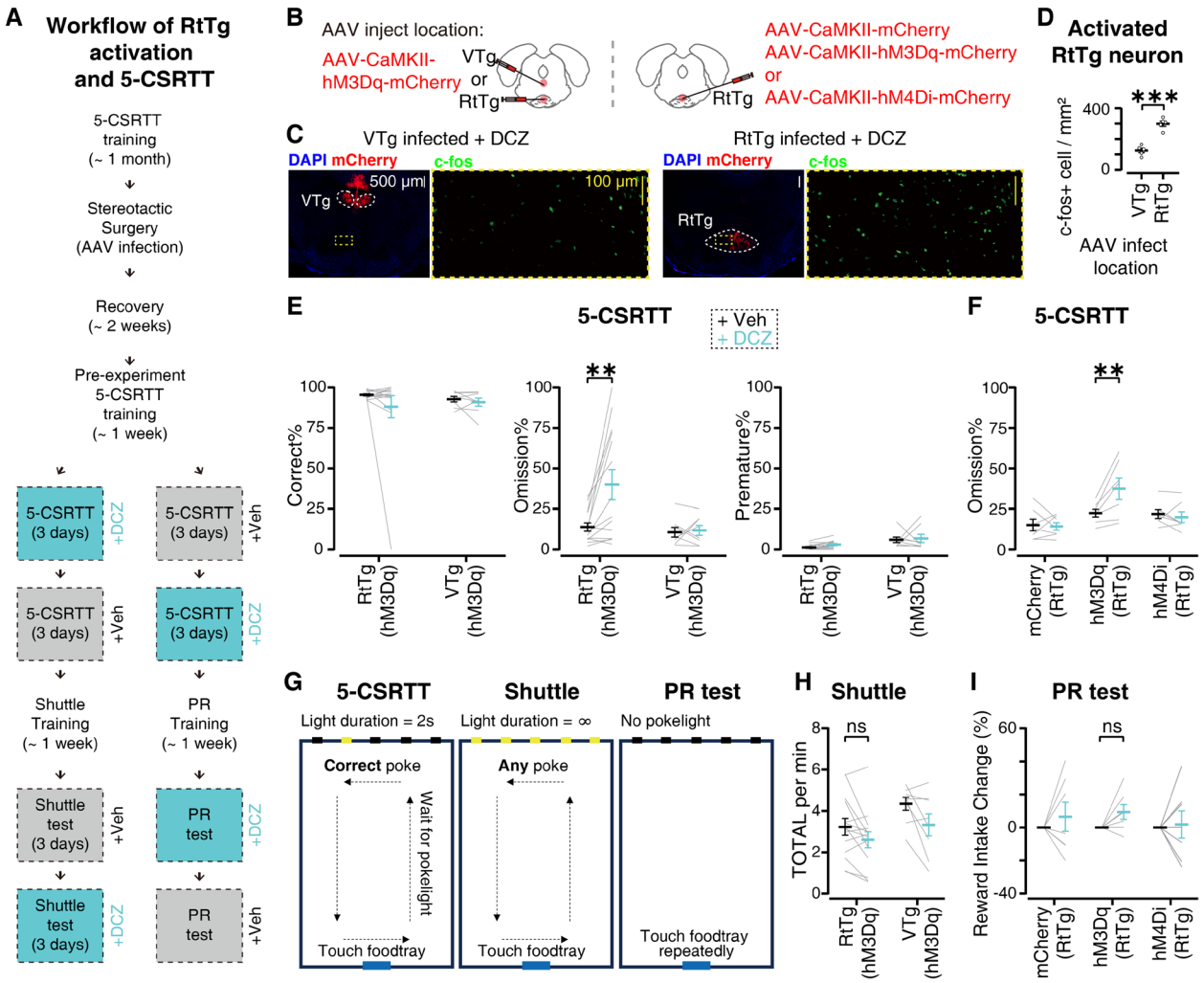

Fig. 5 Activation of RtTg neurons induces attention deficits. **A** Workflow of chemogenetic RtTg activation and behavior tests. **B** Left: Schematic representation of the injection site for AAV2/9-mCaMKIIa-hM3Dq-mCherry-WPRE-ER2-pA (AAV-hM3Dq or hM3Dq) with the ventral tegmental nucleus (VTg) used as a control injection site. Right: Schematic representation of the injection site for AAV-hM3Dq and the control virus AAV2/9-mCaMKIIa-mCherry-WPRE-ER2-pA (mCherry) and AAV2/9-mCaMKIIa-hM4Di-mCherry-WPRE-ER2-pA (hM4Di). **C** IF of AAV-infected site and neuronal activation marker c-fos. **D** Statistics of activated RtTg neurons after DCZ injection (n = 5 per group, ***$p < 0.001$, unpaired *t*-test). **E** 5-CSRTT performance of RtTg or VTg AAV-hM3Dq infected rats, showing results consistent with those observed after METH treatment (RtTg infected group: n = 14; VTg infected group: n = 8, *$p < 0.05$; **$p < 0.01$, 2-way ANOVA with Bonferroni correction). **F** 5-CSRTT performance of RtTg AAV-mCherry, AAV-hM3Dq or AAV-hM4D infected rats (n = 7 per group, **$p < 0.01$, 2-way ANOVA with Bonferroni correction). **G** Schematic of behavior tests. The Shuttle test is a simplified version of the 5-CSRTT, designed to mimic the movement required in 5-CSRTT. The Reward Desire Test is a classical progressive ratio (PR) test conducted within the 5-CSRTT instrument. **H** Shuttle test performance of RtTg or VTg AAV-hM3Dq infected rats, with TOTAL representing the total initiated trail, identical to the 5-CSRTT (RtTg infected group: n = 14; VTg infected group: n = 8; ns, $p > 0.05$, 2-way ANOVA with Bonferroni correction). **I** Progressive ratio test performance of RtTg AAV-mCherry, AAV-hM3Dq, or AAV-hM4D infected rats. Reward intake change = (Reward intake_{DCZ} – Reward intake_{Veh})/Reward intake_{Veh} (n = 7 per group, ns, $p > 0.05$, 2-way ANOVA with Bonferroni correction)

$p > 0.999$). These results indicate that the changes in 5-CSRTT parameters resulting from RtTg neuron activation mimic those observed with METH exposure, particularly in terms of Omission%, while Correct% and Premature% remain unaffected.

RtTg neurons have been implicated in forelimb movement regulation [48] and serves as a source of cerebellar mossy fibers associated with reward-seeking motivation [49]. Impairments in locomotion or motivation could potentially result in increased omission responses, confounding the measurement of attention deficits. To rule out such confounding effects, we conducted a Shuttle test to simulate the movement required in the 5-CSRTT. In this test, rats shuttled between a nose-poke port and

a food tray to receive rewards, with no time constraints or requirements for correct/error judgments (Figs. 5G, S5B for workflow). The results showed no significant difference in TOTAL after RtTg activation in the hM3Dq group ($p=0.100$, Fig. 5H), suggesting that RtTg activation did not impair the basic shuttle movement abilities required for the 5-CSRTT. Furthermore, we assessed the effect of RtTg neuron activation on reward-seeking motivation using the PR test. Results showed no significant difference in motivation after RtTg activation ($p=0.670$, Fig. 5I), indicating that activation of RtTg neurons did not affect the rats' motivation to obtain rewards.

These findings demonstrate that selective activation of RtTg neurons can reproduce METH-like attention deficits in rats that have not been exposed to METH. Taken together, our results suggest that METH-induced attention deficits are critically dependent on the activity of RtTg neurons.

Discussion

This study provides significant insights into the cellular mechanisms underlying METH-induced attention deficits by highlighting the critical role of RtTg. Through single-nucleus RNA sequencing and immunofluorescence, we demonstrated that chronic METH exposure induces aberrant gene expression in RtTg neurons, particularly affecting glutamatergic synapses and increasing neuronal activity. Crucially, our experiments show that selective chemogenetic inactivation of these neurons or RtTg lesions mitigated METH-induced attention deficits, while their activation reproduced these deficits in METH-naive rats. These findings underscore the RtTg as a promising therapeutic target for addressing attention deficits associated with METH use.

Our results align with prior studies on amphetamine-induced attention impairments, particularly the more pronounced increase in Omission% compared to the decrease in Correct% [28, 50]. Similar trends have been observed with METH, further validating our experimental approach [16, 18]. By replicating these classical findings, we confirm that our METH injection protocol successfully induces attentional deficits. Previous research suggests that distinct brain regions regulate different aspects of attention [20], and recent studies have posited that Correct% and Omission% reflect separate attentional states [51]. Consistent with this, we observed that RtTg activation selectively increased Omission% without significantly affecting Correct%, in contrast to the anterior cingulate cortex (ACC), where METH mainly reduces Correct% without altering Omission% [52, 53].

The RtTg is an essential node in the cortico-cerebellar circuit and has been linked to various cognitive processes, including fear [54], startle [55], and associative learning [56]. Our study adds to this body of research by implicating the RtTg in the regulation of attention. This supports the glutamate hypothesis, which posits that METH impairs cognitive functions through dysregulation of glutamate release [57, 58].

The frontal cortex is well-known for its critical role in attention regulation [11, 31, 59]. Given that attention regulation involves the integration of complex information [60], other regions associated with the frontal cortex may also contribute to drug-induced alternations in attention. The RtTg is located within the cortico-cerebellar projection, receiving cortical signals and transmitting them to the cerebellum [13]. Previous studies have demonstrated RtTg is active in attention-related tasks such as eye movement control [15, 61], and cerebellar lesions impair attentional performance by disrupting time-sensing abilities [62]. Abnormal RtTg activation may distort the transmission of attentional control signals from the frontal cortex to the cerebellum, leading to increased omissions in the 5-CSRTT.

As limitations, we studied only male rats to avoid hormonal confounds, thereby restricting our conclusions to male subjects. Including both sexes in future research will be important to explore potential sex differences in METH-induced attention deficits. Further studies employing electrophysiology and circuit tracing with AAV infection are essential to identify the RtTg's specific role in encoding attention-related regulatory signals. Additionally, the use of transgenic models will be necessary to pinpoint the key molecular pathways that mediate METH-induced changes in RtTg function.

While the 5-CSRTT primarily measures visual attention, human attention spans a broader array of cognitive functions relevant to everyday life. The extent to which RtTg neurons regulate other attentional capacities remains unexplored. Additionally, future research should investigate the RtTg's role in learning processes linked to attention. Beyond behavioral analyses, it will be essential to explore the circuit and molecular mechanisms driving RtTg function to deepen our understanding of METH-induced cognitive impairments.

Conclusion

This study demonstrates that the RtTg neuron is essential for METH-induced attention deficits. We believe that RtTg inactivation is a promising therapeutic strategy for further application.

Abbreviations

5-CSRTT	5-Choice serial reaction time task
AAV	Adeno-associated virus
ANOVA	Analysis of variance
BPN	Basilar pontine nuclei
DAPI	4′,6-Diamidino-2-phenylindole
DCZ	Deschloroclozapine
DREADD	Designer receptors exclusively activated by designer drugs
IF	Immunofluorescence
ISH	In situ hybridization
KEGG & GO	Kyoto Encyclopedia of Genes and Genomes and Gene Ontology
METH	Methamphetamine
NFIB	Nuclear factor I/B
PN	Pontine nuclei
PR test	Progressive ratio test
RtTg	Reticulotegmental nucleus
snRNA-Seq	Single-nuclei RNA sequencing
Veh	Vehicle
VGLUT	Vesicular glutamate transporter
VTg	Ventral tegmental nucleus

Supplementary Information

The online version contains supplementary material available at https://doi.org/10.1186/s40478-024-01890-0.

Additional file 1.

Additional file 2.

Additional file 3.

Additional file 4.

Additional file5 (DOCX 15489 KB)

Acknowledgements

We thank Dr. Jing Zhang for METH safety and laboratory affairs, Dr. Bing Lu and Dr. Xuewen Cheng for manuscript revision and guidance on molecular and behavioral experiments, and Di Deng, Yingjie Cheng, and Wenlei Zhang from the Shanghai Mental Health Center for assistance with METH treatment in rats. Special thanks to Ling Han from the Institute of Neuroscience for providing behavioral testing, rat surgery, and METH injection facilities. Special thanks to Dr. Min Zhao from the Shanghai Mental Health Center for her invaluable assistance with METH applications and her insightful suggestions on our experimental design.

Author contributions

XTQ, RWZ, and Z-QX designed the experiments. XTQ performed the experiments and analyzed the data. PYY assisted with the rat METH treatment during the snRNA-seq stage. XTQ wrote the manuscripts, and XTQ, RWZ, and Z-QX revised it.

Funding

This work was supported by the Ministry of Science and Technology (2018YFA0801404 to Z-Q. X.), National Natural Science Foundation of China Grant (82021001 to Z-Q.X.), and Shanghai Municipal Science and Technology Major Project.

Availability of data and materials

All data are available in the main text or the supplementary materials.

Declarations

Ethics approval and consent to participate

Animal ethics in this paper were approved by the Institutional Animal Care and Use Committee of the Center for Excellence in Brain Science and Intelligent Technology of the Chinese Academy of Sciences. Academy of Sciences in accordance with national guidelines.

Consent for publication

Not applicable.

Competing interests

The authors declare that they have no competing interests.

Received: 2 October 2024 Accepted: 15 November 2024
Published online: 22 November 2024

References

1. Cruickshank CC, Dyer KR (2009) A review of the clinical pharmacology of methamphetamine. Addiction 104(7):1085–1099
2. Sim T et al (2002) Cognitive deficits among methamphetamine users with attention deficit hyperactivity disorder symptomatology. J Addict Dis 21(1):75–89
3. Salo R et al (2007) Attentional control and brain metabolite levels in methamphetamine abusers. Biol Psychiatry 61(11):1272–1280
4. Nordahl TE, Salo R, Leamon M (2003) Neuropsychological effects of chronic methamphetamine use on neurotransmitters and cognition: a review. J Neuropsychiatry Clin Neurosci 15(3):317–325
5. Choi JK et al (2018) Abstinence to chronic methamphetamine switches connectivity between striatal, hippocampal and sensorimotor regions and increases cerebral blood volume response. Neuroimage 174:364–379
6. Paulus MP et al (2002) Behavioral and functional neuroimaging evidence for prefrontal dysfunction in methamphetamine-dependent subjects. Neuropsychopharmacology 26(1):53–63
7. Bhattacherjee A et al (2019) Cell type-specific transcriptional programs in mouse prefrontal cortex during adolescence and addiction. Nat Commun 10(1):4169
8. Dang J et al (2020) Glial cell diversity and methamphetamine-induced neuroinflammation in human cerebral organoids. Mol Psychiatry 26:1194–1207
9. Avey D et al (2018) Single-cell RNA-seq uncovers a robust transcriptional response to morphine by glia. Cell Rep 24(13):3619–3629
10. Flores-Dourojeanni JP et al (2021) Temporally specific roles of ventral tegmental area projections to the nucleus accumbens and prefrontal cortex in attention and impulse control. J Neurosci 41(19):4293–4304
11. Bari A et al (2020) Differential attentional control mechanisms by two distinct noradrenergic coeruleo-frontal cortical pathways. Proc Natl Acad Sci U S A 117(46):29080–29089
12. Kratochwil CF, Maheshwari U, Rijli FM (2017) The long journey of pontine nuclei neurons: from rhombic lip to cortico-ponto-cerebellar circuitry. Front Neural Circuits 11:33
13. Henschke JU, Pakan JM (2020) Disynaptic cerebrocerebellar pathways originating from multiple functionally distinct cortical areas. Elife 9:e59148
14. Kellermann T et al (2012) Effective connectivity of the human cerebellum during visual attention. J Neurosci 32(33):11453–11460
15. Ono S, Das VE, Mustari MJ (2004) Gaze-related response properties of DLPN and NRTP neurons in the rhesus macaque. J Neurophysiol 91(6):2484–2500
16. Nazari A et al (2020) Age-dependent effects of repeated methamphetamine exposure on locomotor activity and attentional function in rats. Pharmacol Biochem Behav 191:172879
17. Bari A, Dalley JW, Robbins TW (2008) The application of the 5-choice serial reaction time task for the assessment of visual attentional processes and impulse control in rats. Nat Protoc 3(5):759–767
18. Siemian JN et al (2017) Comparison of some behavioral effects of d- and l-methamphetamine in adult male rats. Psychopharmacology 234(14):2167–2176
19. Dalley JW et al (2007) Enduring deficits in sustained visual attention during withdrawal of intravenous methylenedioxymethamphetamine self-administration in rats: results from a comparative study with d-amphetamine and methamphetamine. Neuropsychopharmacology 32(5):1195–1206
20. Bernheim A, See RE, Reichel CM (2016) Chronic methamphetamine self-administration disrupts cortical control of cognition. Neurosci Biobehav Rev 69:36–48

21. Jayanthi S et al (2014) Methamphetamine downregulates striatal glutamate receptors via diverse epigenetic mechanisms. Biol Psychiatry 76(1):47–56
22. Hasan H, et al. Rodent models of methamphetamine misuse: mechanisms of methamphetamine action and comparison of different rodent paradigms. In: Psychiatric disorders methods and protocols. 2019. pp. 221–250.
23. Xie C et al (2011) KOBAS 2.0: a web server for annotation and identification of enriched pathways and diseases. Nucleic Acids Res 39(Web Server issue):W316–W322
24. Schneider Gasser EM et al (2006) Immunofluorescence in brain sections: simultaneous detection of presynaptic and postsynaptic proteins in identified neurons. Nat Protoc 1(4):1887–1897
25. Shihan MH et al (2021) A simple method for quantitating confocal fluorescent images. Biochem Biophys Rep 25:100916
26. Cetin A et al (2006) Stereotaxic gene delivery in the rodent brain. Nat Protoc 1(6):3166–3173
27. Asinof SK, Paine TA (2014) The 5-choice serial reaction time task: a task of attention and impulse control for rodents. J Vis Exp 90:e51574
28. Fletcher PJ et al (2007) A sensitizing regimen of amphetamine impairs visual attention in the 5-choice serial reaction time test: reversal by a D1 receptor agonist injected into the medial prefrontal cortex. Neuropsychopharmacology 32(5):1122–1132
29. Vincent KF et al (2021) Return of the righting reflex does not portend recovery of cognitive function in anesthetized rats. Front Syst Neurosci 15:762096
30. Koike H et al (2016) Chemogenetic inactivation of dorsal anterior cingulate cortex neurons disrupts attentional behavior in mouse. Neuropsychopharmacology 41(4):1014–1023
31. Norman KJ et al (2021) Post-error recruitment of frontal sensory cortical projections promotes attention in mice. Neuron 109(7):1202–1213
32. Kaukas L et al (2021) Effects of remote immune activation on performance in the 5-choice serial reaction time task following mild traumatic brain injury in adolescence. Front Behav Neurosci 15:659679
33. Popik P et al (2022) Effects of ketamine optical isomers, psilocybin, psilocin and norpsilocin on time estimation and cognition in rats. Psychopharmacology 239(6):1689–1703
34. Stuart T et al (2019) Comprehensive integration of single-cell data. Cell 177(7):1888–1902
35. Segal DS et al (2003) Escalating dose methamphetamine pretreatment alters the behavioral and neurochemical profiles associated with exposure to a high-dose methamphetamine binge. Neuropsychopharmacology 28(10):1730–1740
36. Iamjan SA et al (2024) Regional-specific changes in rat brain BDNF in a model of methamphetamine abuse. Neurosci Lett 836:137880
37. Valian N, Ahmadiani A, Dargahi L (2018) Increasing methamphetamine doses inhibit glycogen synthase kinase 3β activity by stimulating the insulin signaling pathway in substantia nigra. J Cell Biochem 119(10):8522–8530
38. Belcher AM et al (2008) Methamphetamine influences on recognition memory: comparison of escalating and single-day dosing regimens. Neuropsychopharmacology 33(6):1453–1463
39. Saunders A et al (2018) Molecular diversity and specializations among the cells of the adult mouse brain. Cell 174(4):1015–1030
40. Schmahmann JD, Ko R, MacMore J (2004) The human basis pontis: motor syndromes and topographic organization. Brain 127(Pt 6):1269–1291
41. Brodal P, Bjaalie JG (1992) Organization of the pontine nuclei. Neurosci Res 13(2):83–118
42. Tziridis K, Dicke PW, Thier P (2012) Pontine reference frames for the sensory guidance of movement. Cereb Cortex 22(2):345–362
43. Wu SR et al (2023) Atoh1 drives the heterogeneity of the pontine nuclei neurons and promotes their differentiation. Sci Adv 9(26):eadg1671
44. Nectow AR et al (2017) Identification of a brainstem circuit controlling feeding. Cell 170(3):429–442
45. Berretta S et al (1991) The cerebellopontine system: an electrophysiological study in the rat. Brain Res 568(1–2):178–184
46. Woo MS et al (2021) Neuronal metabotropic glutamate receptor 8 protects against neurodegeneration in CNS inflammation. J Exp Med 218(5):e20201290
47. Ehrengruber MU et al (1997) Activation of heteromeric G protein-gated inward rectifier K+ channels overexpressed by adenovirus gene transfer inhibits the excitability of hippocampal neurons. Proc Natl Acad Sci U S A 94(13):7070–7075
48. Matsunami K (1987) Neuronal activity in nuclei pontis and reticularis tegmenti pontis related to forelimb movements of the monkey. Neurosci Res 5(2):140–156
49. Kostadinov D, Hausser M (2022) Reward signals in the cerebellum: origins, targets, and functional implications. Neuron 110(8):1290–1303
50. Dalley JW et al (2005) Cognitive sequelae of intravenous amphetamine self-administration in rats: evidence for selective effects on attentional performance. Neuropsychopharmacology 30(3):525–537
51. Vouillac-Mendoza C et al (2024) Knowledge by omission: the significance of omissions in the 5-choice serial reaction time task. Psychopharmacology 241(7):1319–1328
52. van der Veen B et al (2021) Control of impulsivity by G(i)-protein signalling in layer-5 pyramidal neurons of the anterior cingulate cortex. Commun Biol 4(1):662
53. White MG et al (2018) Anterior cingulate cortex input to the claustrum is required for top-down action control. Cell Rep 22(1):84–95
54. Guo W et al (2022) A midbrain-reticulotegmental circuit underlies exaggerated startle under fear emotions. Mol Psychiatry 27(12):4881–4892
55. Guo W et al (2021) A Brainstem reticulotegmental neural ensemble drives acoustic startle reflexes. Nat Commun 12(1):6403
56. Xiao N et al (2023) Positive feedback of efferent copy via pontine nucleus facilitates cerebellum-mediated associative learning. Cell Rep 42(2):112072
57. Kalivas PW (2009) The glutamate homeostasis hypothesis of addiction. Nat Rev Neurosci 10(8):561–572
58. Ohmori T, Abekawa T, Koyama T (1996) The role of glutamate in behavioral and neurotoxic effects of methamphetamine. Neurochem Int 29(3):301–307
59. Kim H et al (2016) Prefrontal parvalbumin neurons in control of attention. Cell 164(1–2):208–218
60. Knudsen EI (2007) Fundamental components of attention. Annu Rev Neurosci 30:57–78
61. Darlington TR, Lisberger SG. Sensory-motor computations in a cortico-pontine pathway. 2022.
62. Breska A, Ivry RB (2020) Context-specific control over the neural dynamics of temporal attention by the human cerebellum. Sci Adv 6(49):eabb1141

Publisher's Note